

<https://doi.org/10.1038/s44431-026-00022-z>

Mechanical anisotropy in compressive-stress shape-programmed liquid crystal elastomers and polymer-dispersed liquid crystal elastomer composites

Check for updates

Marta Lavrič¹, Luka Racman Knez², Valentina Domenici³ & Andraž Rešetic^{1,2}✉

Polymer-dispersed liquid crystal elastomer composites (PDLCEs) combine the thermomechanical capabilities of liquid crystal elastomers (LCEs) with the softness of a silicone matrix. The high-temperature persistent glass phase in LCEs allows preservation of the instilled deformations during thermal cycling, leading to reprogrammable shape-memory in both LCEs and PDLCEs. This provides a unique opportunity to study mechanical properties within a single shape-programmed specimen by imposing different mesogen configurations or particle geometries, without the need for repeated synthesis. We specifically focus on compressive programming, which induces transverse mechanical anisotropy and a mesogen configuration with a negative order parameter. Directional stress–strain and thermomechanical tests reveal that, despite the elastic matrix, PDLCEs retain mechanical properties comparable to pure LCEs, highlighting the role of mechanical anisotropy together with inclusion alignment and geometry. The degree of mesogen ordering is evaluated in LCEs, while a modified Halpin–Tsai model captures the mechanical response of PDLCEs.

Due to their thermomechanical (TM) properties and shape-changing capabilities, liquid crystal elastomers¹ (LCEs) and their composite counterparts, polymer-dispersed liquid crystal elastomers^{2,3} (PDLCEs), are promising candidates for implementation in future devices as soft smart materials^{4–6}. Their actuation capabilities originate from the order–disorder transition of their liquid crystal molecular components, or mesogens, triggered either by light irradiation or changes in temperature¹.

In addition to their reversible TM actuation, which is intrinsic to the ordering instilled during LCE preparation, the shape of LCEs can also be reprogrammed by various methods^{7,8}. One approach involves the use of light- or temperature-sensitive reversible bonds that, once activated, re-crosslink the reshaped LCE network into a new geometry, from which it can then actuate reversibly until the bonds are dissociated by a similar stimulus^{9,10}. Another method exploits the temperature-dependent glassiness of the LCE polymer network, allowing the material to be fixed into a temporary shape at low temperatures and to irreversibly relax back to its original form once heated above the glass phase^{2,11,12}—a mechanism widely employed in shape-memory polymers¹³.

In all cases, such manipulations involve deforming the sample into a new shape, which introduces additional ordering into the LCE network and

reorients the mesogens along the direction of the applied mechanical field. As a result, the material can become highly anisotropic in the ordered state, affecting not only the magnitude and direction of TM deformation, but also its mechanical properties, which now depend on the orientation of the applied stress relative to the imprinted mesogen and polymer network alignment¹.

A similar situation is observed in PDLCEs, which are composed of dispersed LCE microparticles embedded in a soft silicone matrix^{2,3}. In such composites, the actuating properties of the LCE microparticles, once orientationally ordered so that their mesogen alignment faces the same direction, are transferred to the entire PDLCE, enabling TM actuation³. Moreover, other similar TM properties are inherited by the composite as well, including shape-memory behavior². PDLCEs can therefore be reshaped by taking advantage of the glassy behavior of the LCE inclusions, enabling a new shape to be imprinted under constant stress during thermal cycling. The process involves heating the sample so that the inclusions soften and deform under stress; as the composite cools back into the glass phase, they solidify and lock in the new shape.

While one of the key characteristics of LCEs is their TM anisotropy, it would be beneficial for many applications to develop a soft smart material

¹Jožef Stefan Institute, Solid State Physics Department, Jamova Cesta 39, 1000 Ljubljana, Slovenia. ²Faculty of Polymer Technology, Ozare 19, 2380 Slovenj Gradec, Slovenia. ³Dipartimento di Chimica e Chimica Industriale, Università degli studi di Pisa, via Moruzzi 13, 56124 Pisa, Italy. ✉ e-mail: andraz.resetic@ijs.si

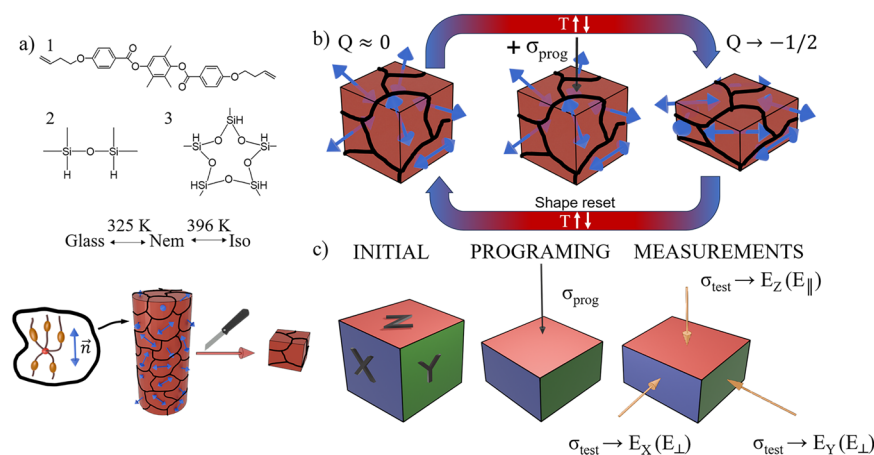


Fig. 1 | MC-LCE composition and schematic of the programming and measuring process. **a** MC-LCEs are comprised of a polymer network made of divinyl terminated main-chain monomers (1), polymer chain extenders (2) and crosslinked with five-point crosslinkers (3). MC-LCEs were synthesized as a bulk, polydomain system, from which cube-shaped samples were cut. Phase transition temperatures are based on ac calorimetry measurements performed in our previous study².

b Programming of the sample is carried out by thermal cycling to and from the isotropic phase while maintaining a programming stress. The programmed shape can then be reset to the original geometry by another thermal cycle without an applied load. **c** For the experiments, the sample was shape-programmed in one direction and then measured from all three to yield the associated Young's moduli, E_{\parallel} and E_{\perp} with respect to the programming stress.

that can retain its mechanical properties independently of the internal anisotropy required for actuation. PDLCEs hold that potential, due to the presence of a soft, elastic, and TM-isotropic silicone matrix, which can suppress the influence of the embedded LCE material. However, we will show that this suppression is limited, as the mechanical anisotropy in PDLCEs is significantly affected by the geometrical changes of shape-programmed inclusions.

The mechanical anisotropy of LCE materials with uniaxially aligned mesogen order has already been extensively studied and is well understood^{14–21}. In contrast, far fewer studies have addressed anisotropy induced via compressive stress^{22–25}. Compressive stress produces transverse mesogen alignment relative to the loading direction, resulting in a negative order parameter that is not trivial to achieve with tensile programming²⁶. The role of the negative order parameter in LCEs and PDLCEs could be relevant not only from a mechanical perspective, for instance, in stress dissipation or directional material stiffening^{27,28}, but also from an optical standpoint²⁹. In the context of 3D shape programming, compressive stress naturally occurs in many geometries and provides a straightforward means of programming such materials. Understanding its effect is therefore necessary to clarify the TM response of both LCEs and PDLCE composites, as it can also lead to actuation behavior not accessible with tensile programming alone. Experiments under compressive loading are relatively uncommon, as most work in the field has focused on thin-film LCE geometries. Bulk LCE systems produced via additive manufacturing represent an exception, although their mechanical behavior depends on a complex interplay between mesogen alignment and printing parameters, such as deposition direction and layer orientation^{30–32}.

To clarify the mechanisms behind the observed mechanical anisotropy, we investigate the TM mechanical behavior of both PDLCEs and their LCE counterparts, first to quantify and control the level of TM anisotropy achieved through shape programming, and second, to identify the underlying contributions from mesogen ordering in both systems and from particle geometry in PDLCEs. The experimental results are further analyzed by applying existing theoretical models. The negative order parameter in LCEs is estimated from directional modulus measurements, while the Halpin–Tsai model, used to predict the mechanical properties of polymer composites with anisotropic inclusions, is applied to evaluate the influence of particle geometry on the mechanical response of PDLCEs.

Results

Main-chain liquid crystal elastomers

Shape reprogramming in the MC-LCEs presented here is enabled by a high-temperature glass phase, where thermally induced dissolution and recrystallization of crystallites significantly modify the mechanical properties of the material (Fig. 1). As the temperature changes from the glass phase to the nematic phase, tensile tests in our previous study³ showed that the associated Young's modulus decreases by nearly two orders of magnitude, from $E_{\text{glass}} \rightarrow \text{GPa}$ to $E_{\text{nem}} \rightarrow \text{kPa}$. This enables deformation of the material at elevated temperatures and imprints the imposed strain by fully arresting relaxation upon cooling below the glass-to-nematic phase transition. This also leads to an 'on-demand' imprinting of material anisotropy and provides the opportunity to study mechanical properties with respect to the internal molecular arrangement, albeit in the glass phase. Since the new molecular configuration remains frozen until reset at a higher temperature, the direction of anisotropy can be chosen during programming and subsequently measured along any desired direction.

In order to assess the mechanical anisotropy in LCEs, we synthesized an irregular piece of polydomain MC-LCE material with an approximate volume of 1 cm³, from which we cut a cube-shaped sample (Fig. 1a; see also "Methods"). The geometry of the sample allowed for directional shape programming under a constant compressive load (Supplementary Fig. 1). A compressive deformation of approximately $\lambda_{\text{nem}} \approx 0.40$ was imprinted in the sample, and the Young's modulus was measured in all three directions (Fig. 1b, c). We define the deformation parameter as $\lambda = 1 + \epsilon$, where $\epsilon = \Delta L/L_0$ is the elastic strain, measured from the ratios of the length change ΔL and the initial length L_0 . After each experiment, the sample's shape was reset by heating to the isotropic state, reprogrammed in a different direction, and the measurements were repeated.

The results shown in Fig. 2a present a significant drop in Young's modulus in the parallel direction to the programmed strain (E_{\parallel}), i.e., measured when $\sigma_{\text{test}} \parallel \sigma_{\text{prog}}$, while an increase in the modulus in the perpendicular directions (E_{\perp}), i.e., when $\sigma_{\text{test}} \perp \sigma_{\text{prog}}$, is observed. The moduli are normalized with the respective E_0 values of the non-programmed sample to account for the initial variations in E between the three directions of the MC-LCE cube. Non-normalized values can be found in Supplementary Fig. 2. The decrease in the parallel directions is similar for all three configurations, with the average value of $E_{\parallel}/E_0 \approx 0.43$. Correspondingly, the perpendicular component rises on average to about $E_{\perp}/E_0 \approx 1.17$. Here, the values exhibit larger variations, mostly due to the non-ideal

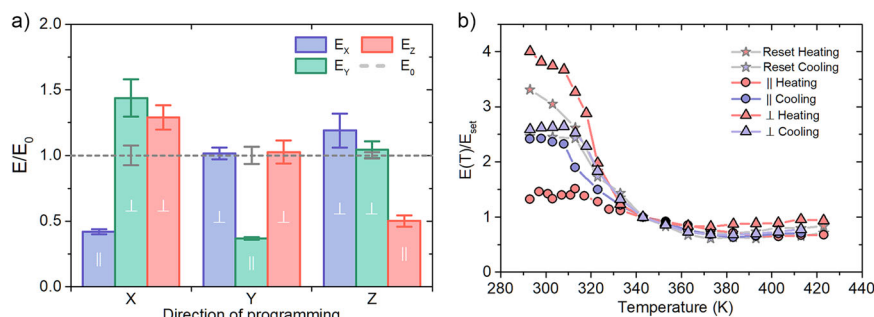


Fig. 2 | Anisotropic Young's moduli of a shape-programmed MC-LCE and temperature relaxation of mechanical anisotropy. **a** The graphs show the normalized Young's modulus values for each programmed configuration, i.e., programmed perpendicular to the X, Y, and Z surfaces. The error bars are significantly smaller in the programmed direction due to good contact between the holders and the sample surface, which conformed to the holders during shape programming.

b Young's modulus as a function of temperature is shown for the relaxed and shape-programmed MC-LCE in the parallel and perpendicular directions against the programmed surface. For clearer comparison, the moduli are normalized to the E_{set} value measured at $T_{set} = 343$ K, i.e., the synthesis temperature of the material, where no internal stresses are expected to be present. The profiles were measured during both heating and cooling runs.

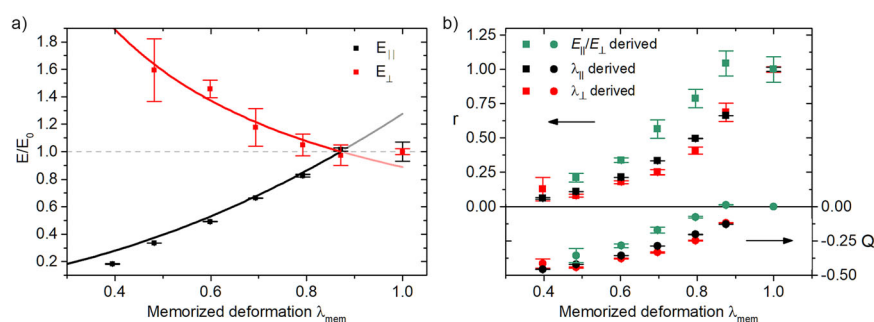


Fig. 3 | Instilled mechanical and mesogen order anisotropy in a shape-programmed MC-LCE. **a** The $E_{||}$ and E_{\perp} moduli diverge significantly with increasing memorized deformation, with $E_{||}$ decreasing and E_{\perp} increasing. The lines represent values calculated from Eq. (1) and show good agreement with the experimental results. The parameters used in the calculation were obtained from measured material properties, $E_{||}^0 = 14.06$ MPa and $E_{\perp}^0 = 8.37$ MPa, and with

$\nu = 0.5$. **b** Step-length anisotropy r is obtained from the measured Young's moduli (green squares), calculated using Eq. (2), and from the parallel and perpendicular memorized deformations (black and red squares, respectively), via the relations $\lambda_{||} = r^{1/3}$ and $\lambda_{\perp} = r^{-1/6}$. The graph also shows the corresponding order parameter Q (right side values). In all cases, r and Q decrease with increasing memorized deformation, with some deviations between r_E , Q_E and r_{λ} , Q_{λ} .

contact between the thinner shape-programmed sample and the holders. Nevertheless, the significant changes in $E_{||}$ and E_{\perp} values indicate the formation of an ordered system from the initial polydomain MC-LCE.

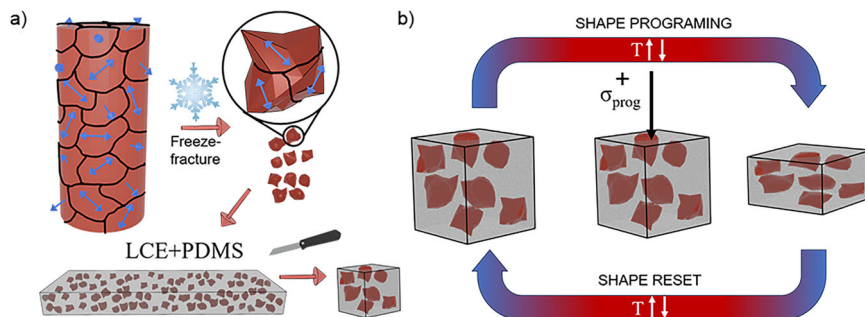
The effect can be reversed by heating the sample. The graph in Fig. 2b shows the evolution of the measured Young's moduli of the shape-programmed and non-programmed MC-LCE with temperature. The memorized strains are completely reset once heated above the nematic to isotropic phase transition (see also Supplementary Fig. 1), while the anisotropy in the Young's modulus in both directions vanishes above 330 K, where all $E(T)$ curves begin to follow similar behavior. This temperature coincides with the transition temperature from the glassy to the nematic phase of the material². After cooling, the sample consistently returns to its polydomain state, although in this experiment it settles slightly below the initial, non-deformed value (Fig. 2b, red stars).

Further tests demonstrate that the extent of mechanical anisotropy is also reflected in the amount of strain programmed into the MC-LCE material (Fig. 3). Here, the modulus of the programmed sample remains isotropic in both direction ($E_{prog}/E_0 \approx 1$) at lower memorized deformation, $\lambda_{mem} < 0.90$, after which the $E_{||}$ and E_{\perp} moduli begin to diverge with increasing memorized compressive strain. This strain corresponds to the known threshold at which polydomain LCE systems begin to reorient their LC domains along the direction of applied uniaxial tensile stress, resulting in increased mesogen order in that direction¹. This reorientation also renders the material's properties anisotropic, with a higher modulus when measured parallel and a lower modulus when perpendicular to the mesogen alignment^{14–17}.

In our case, the mesogens are forced into a transverse configuration by the applied compressive stress (Fig. 1c). Such alignment is associated with a negative mesogen order parameter Q , where $Q = -1/2$ represents a complete in-plane distribution of mesogens, relative to the chosen director \mathbf{n} . A direct observation of a negative Q as the consequence of applied compressive stress has been reported in a polymer network²⁸, while theoretical studies of compressive deformation in monodomain LCEs have shown the formation of lamellar domains under increasing stress³³, consistent with mesogen arrangements characterized by a negative order parameter. We can likewise estimate the imprinted negative order parameter Q by evaluating the step-length anisotropy r from the measured mechanical properties of the sample, as described below.

In terms of polymer chain conformation, the LCE's molecular configuration is characterized by the step length anisotropy $r = l_{||}/l_{\perp}$, which describes the ratio between the parallel and perpendicular components of the step length tensor $\underline{l} = \text{Diag}(l_{\perp}, l_{\perp}, l_{||})$. This tensor reflects the current nematic ordering in the LCE network as determined by the effective step length of the polymer chain's random walk¹ (Supplementary Fig. 3). When $r = 1$, the polymer chain conformation is spherical ($l_{||} = l_{\perp}$), and the material is isotropic, exhibiting no directional thermal deformation. For $r > 1$, the network adopts a prolate configuration ($l_{||} > l_{\perp}$), while $r < 1$ indicates an oblate configuration ($l_{||} < l_{\perp}$). As a result, the material undergoes spontaneous thermal contraction (for $r > 1$) or elongation (for $r < 1$) along the direction $l_{||}$ upon heating, with the amplitude of deformation given by $\lambda = r^{1/3}$. Since the LCE block in our experiments initially exhibits an isotropic or polydomain state with no predefined nematic director, we

Fig. 4 | PDLCE composition and shape-programming. **a** PDLCEs are composed of non-oriented MC-LCE microparticles embedded in a silicone polymer matrix. **b** Such non-aligned PDLCEs do not exhibit any reversible TM actuation, similar to their polydomain MC-LCE counterparts. However, the shape-memory properties are still conveyed to the composite.



assign a reference direction parallel to the programming stress ($l_{||} || \sigma_{prog}$). Accordingly, the shape programming under compressive stress transforms the network from a spherical to an oblate configuration, i.e., from $r = 1$ to $r < 1$ (Supplementary Fig. 3).

The step-length anisotropy r can thus be determined directly from $\lambda = r^{1/3}$, where $\lambda = L_0/L_{iso}$ is the reversible spontaneous relaxation, calculated from temperature relaxed (L_0) thickness and the sample length in the isotropic phase (L_{iso})¹. For a compressive stress shape-programmed material, this would be the stretch parameter describing the temperature induced relaxation between the programmed shape (L_{mem}) and the isotropic state of the sample, $\lambda_{mem} = L_{mem}/L_{iso}$. Since our sample is polydomain, it exhibits no overall anisotropy ($r = 1$) in the relaxed state, meaning that $L_{iso} \approx L_0$. The material's maximum contraction during heating to the isotropic phase is indeed minimal ($\lambda(T = 410 \text{ K}) \approx 1.025$, Supplementary Fig. 1) and can be safely neglected. The anisotropy r related to the shape-programming of the sample can therefore be calculated from the total relaxation of the programmed memorized strain, $\lambda_{mem} = L_{mem}/L_0$, determined from the room-temperature measurements of the memorized and the initial, temperature relaxed length. By assuming a shear free deformation, $\underline{\lambda} = \text{Diag}(\lambda_{\perp}, \lambda_{\perp}, \lambda_{||})$, and material incompressibility, $\lambda_{||} = 1/\lambda_{\perp}^2$, the parameter r can also be separately determined from the $\lambda_{||}$ and λ_{\perp} measurements.

Besides the TM response, polymer chain anisotropy is also evident in the different mechanical properties along and perpendicular to the polymer network alignment. In our case, the anisotropy r can be derived from the changes in Young's modulus of the initial and shape-programmed LCE block based on to the imposed shape-programmed deformation. The theoretical background for obtaining the anisotropic stretch moduli of an ordered LCE material is well described in ref. 34, and we specifically adopt these calculations, originally derived for the tensile stretch moduli of an ordered LCE block, and apply them to our case. The modified approach is summarized in Supplementary Text 1. In summary, because our system relaxes from a programmed, ordered state back to a polydomain configuration, the spontaneous thermally induced deformation must be treated as the reverse of the typical isotropic-to-nematic transition.

For small compressive strains, where $\lambda \rightarrow 1$, the two stretch moduli components of a shape-programmed LCE system are therefore expressed as:

$$E_{||} = E_{||}^0 \lambda^2 \text{ and } E_{\perp} = E_{\perp}^0 \lambda^{-2\nu} \quad (1)$$

where $E_{||}^0$ and E_{\perp}^0 are the Young's moduli of a non-programmed polydomain LCE, ν is the Poisson ratio and $\lambda \equiv \lambda_{||}$ is the stretch parameter associated with the temperature relaxation from the programmed to the initial length of the material, measured in the direction of the programming stress. A clear distinction between $E_{||}^0$ and E_{\perp}^0 is made here, due to the discrepancies between the measured moduli of the non-programmed LCE (Supplementary Fig. 4). As seen in Fig. 3a (black and red lines), the two calculated moduli match well with the measured values, although the calculations had to be shifted to exclude the data below the non-programmable strain of $\lambda_{prog} > 0.90$ (transparent lines), where the system

remains isotropic – a condition not accounted for by Eq. (1). The transparent lines are the continuation of the theoretical curve beyond this onset and are only indicative.

For an incompressible material, where $\nu = 1/2$, the step length anisotropy can now be determined from the ratios between the compressive moduli of the non- and shape-programmed LCE material:

$$\frac{E_{||}}{E_{\perp}} = \frac{E_{||}^0}{E_{\perp}^0} \lambda^3 = \frac{E_{||}^0}{E_{\perp}^0} r \quad (2)$$

Knowing the value of the anisotropy ratio allows us to further determine the order parameter¹:

$$Q = \frac{r - 1}{r + 2} \quad (3)$$

The evaluations for the step length parameter r and order parameter Q are presented in Fig. 3b as a function of the imprinted deformation λ_{mem} and grouped based on their derivation, either from the measured moduli ratio (r_E, Q_E —green squares) or from the programmable deformation relaxation (r_{λ}, Q_{λ} —red and black squares). Results show that increasing memorized strain reduces r and realigns the system toward a configuration with an increasingly negative order parameter. While the overall trend is consistent between the two methods, r_E and Q_E remain constant for deformations $\lambda_{mem} > 0.90$, where no mesogen alignment is expected, consistent with the typical 10% strain threshold for domain reorientation¹. This behavior is not reflected in the r_{λ} and Q_{λ} values, likely because the glass phase of the system locks the specimen in the deformed configuration before any domain reorientation occurs. This suggests that the strain-derived parameters may not accurately capture the mesogenic ordering.

Overall, the very low values of $r_{E,\lambda} \Rightarrow 0.1$ and $Q_{E,\lambda} \Rightarrow -0.45$ at $\lambda_{mem} = 0.4$ suggest an almost entirely transverse mesogen distribution. Similar values were reported in the literature²⁶ for a thin nematic monodomain system, where perpendicular stretching relative to the director enabled an in-plane reorientation of the nematic domains toward a negative order parameter. More related to our case, modeling of an LCE under compressive stress³³ show the formation of transversely ordered lamellar domains that are localized at the center of the sample. Since we measure the bulk mechanical properties of the entire specimen, we suggest that the extracted r_E and Q_E values probably capture such a lamellar configuration, thus providing a more realistic representation of mesogen ordering. Further analysis, for instance with NMR^{28,35} or XRD measurements²⁵, could offer a deeper insight into the local ordered state of the material.

Polymer-dispersed liquid crystal elastomers

When MC-LCE material is used as micro-inclusions in PDLCEs, they act as microscopic, temperature-dependent hardeners (Fig. 4). This means that PDLCEs can be shape-programmed in the same manner as the parent MC-LCE material, because the MC-LCE microparticles prevent relaxation of the deformed composite system once cooled back to the non-programmable

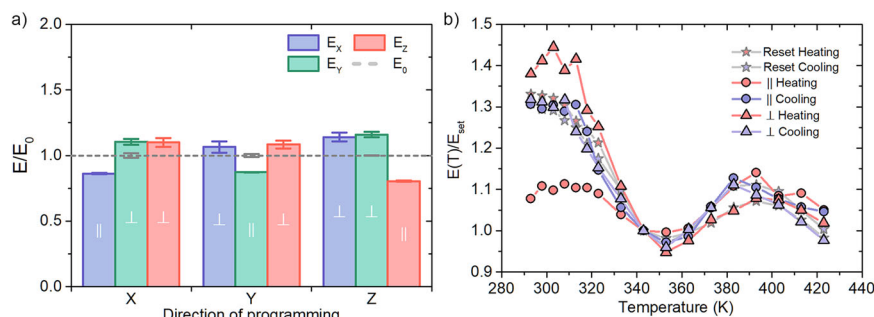


Fig. 5 | Anisotropic Young's moduli of a shape-programmed PDLCE composite and temperature relaxation of mechanical anisotropy. **a** The extent of mechanical anisotropy after shape programming is significantly reduced in PDLCEs, but the trend, i.e., reduced $E_{||}$ and increased E_{\perp} remains the same as in MC-LCEs. The reprogrammability of the material is also preserved by the composite. Additionally, a significant reduction in measurement error is observed, attributed to improved

contact between the PDLCE and the holder surfaces due to the softer and elastic nature of the composite. **b** The mechanical anisotropy fully disappears after each thermal reset of the PDLCE material. Heating curves become comparable after 343 K, which corresponds to the sample preparation temperature and also fall well within the nematic phase of the material. The moduli are also normalized at this temperature.

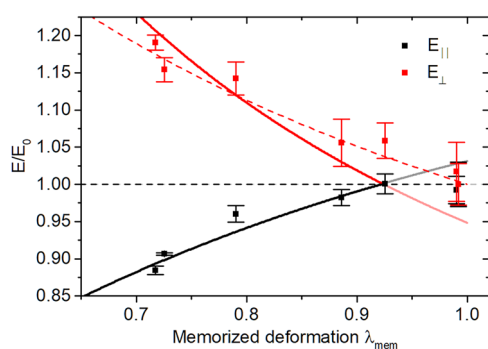


Fig. 6 | Instilled mechanical anisotropy in a PDLCE composite at $w_{LCE} = 0.40$. The $E_{||}$ and E_{\perp} follow a similar trend to those in the pure MC-LCE material—lower $E_{||}$ and higher E_{\perp} with increasing memorized deformation. The Halpin–Tsai evaluation of the effect of LCE particle geometry on mechanical anisotropy is shown with dashed lines. Solid lines represent the same Halpin–Tsai model with additional consideration for the shape-memory induced anisotropy in the Young's modulus of the LCE microparticles (Eqs. (8) and (9)). The results are normalized with the Young's modulus value of the non-programmed specimen.

glass phase². The shape-programming properties are thus transferred onto the PDLCE.

Because of the 3D solid geometry in which PDLCE composites can be molded, compressive stress can be applied without significant issues. The same type of experiment as conducted for the MC-LCE cube was performed on a similarly sized PDLCE cube, in order to assess the extent of preservation of the parent material's properties, as well as to determine the role of the TM inert matrix and the particulate nature of the inclusions on the overall TM properties of the composite.

Figure 5a shows the effect of shape-memory on the Young's modulus on all three sides of the programmed PDLCE cube. The composite was programmed with the same programming deformation as the MC-LCE material ($\lambda_{prog} \approx 0.40$). Overall, the mechanical behavior is mimicked by the composite, with a decrease in the modulus on the programmed side and an increase in the transverse directions. The extent of these changes is significantly lower compared to the MC-LCE—the PDLCE material retains approximately $\lambda_{mem} \approx 0.80$, while the increase on the opposite sides is somewhat comparable to that of the MC-LCE ($\lambda_{\perp} \rightarrow 0.20$). The thermal relaxation of the programmed stress (Fig. 5b) also mimics the behavior of the original material, with an exception of a pronounced maximum observed at $T \approx 395$ K, which corresponds to the LCE's N–I transition temperature found at $T_{N-I} = 396$ K (see Fig. 1a). In all shape-

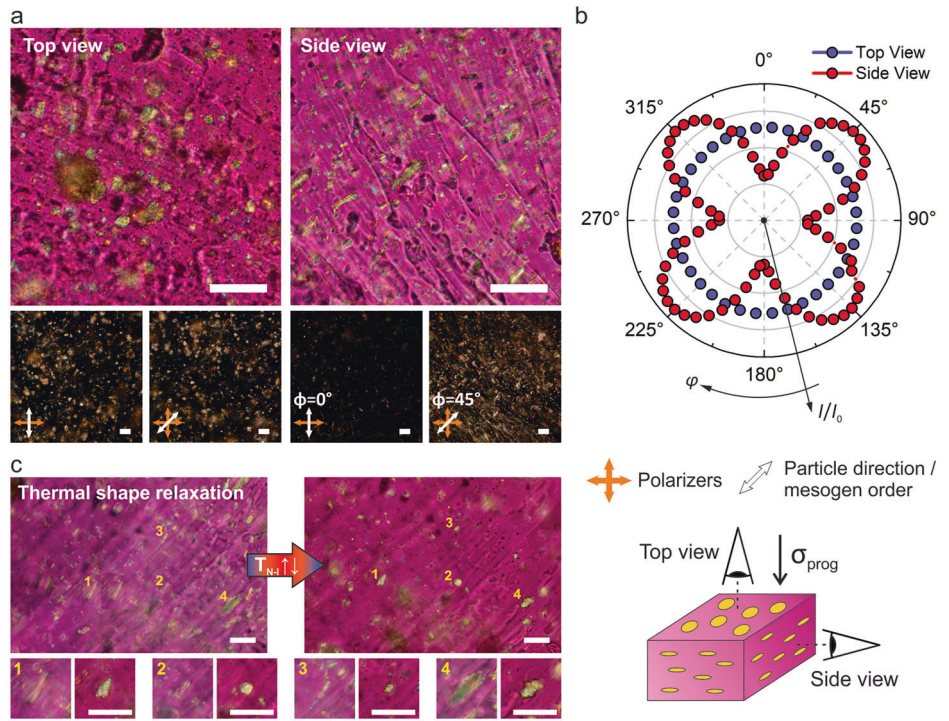
programming scenarios, the material is seen to always relax back to the original dimensions.

The decrease in the anisotropy of mechanical properties is expected, since 60 wt% of the composite is comprised of an elastic silicone matrix with no shape-memory properties. This also accounts for the much lower memorized deformation compared to the programming deformation ($\lambda_{mem} \approx 0.80$ versus $\lambda_{prog} \approx 0.40$). In MC-LCEs, almost all of the programming deformation is preserved by the LCE material. Despite these differences, the transverse mechanical properties remain comparable between the two materials.

This is also seen more clearly when the PDLCE composite is progressively shape-programmed (Fig. 6 and Supplementary Fig. 4). With increasing memorized deformation, a growing divergence between the normalized $E_{||}$ and E_{\perp} from a common initial value is observed, following a trend similar to that seen in the MC-LCE material. The influence of the TM inert matrix is further evident in the saturation of the memorized strain. Even though the maximum programming deformation was $\lambda_{prog} = 0.40$, the PDLCE memorized deformation seems to saturate close to $\lambda_{mem} \rightarrow 0.70$. A notable mechanical anisotropy is only observed at $\lambda_{mem} \approx 0.97$ (corresponding to $\lambda_{prog} = 0.80$), indicating that the soft matrix limits mechanical manipulation of the LCE microparticles, preventing significant changes in their Young's modulus or geometry that would affect the composite's mechanical response. Nonetheless, as noted earlier, while $E_{||}$ is sufficiently suppressed by the matrix, the E_{\perp} values remain comparable to those of the parent material (see Fig. 3a). This suggests that another mechanism, beyond the shape retention of individual particles, contributes to the comparable strain response.

Since the MC-LCE microparticles clearly retain the shape-memory characteristics of the parent material, their geometry is also altered and memorized following TM manipulation. We have previously shown that even nominal applied stress, such as that generated by simple shear flow during thermal cycling, is sufficient to reshape the particles into elongated structures³⁶. In the current experiments, which involve much greater stress, the polarizing optical microscopy (POM) images show that the particles undergo a comparable shape transformation, changing from their initially isotropic, approximately spherical shape into ellipsoidal, disk-like forms (Fig. 7). The top and side views further show that the LCE particles adopt a transverse mesogen orientation, i.e., a negative order parameter Q : no light polarization is observed from the top view in any direction, while the side view clearly shows polarization along the disk plane (Fig. 7a and Supplementary Fig. 5). The changes in the measured sample's transmittance illustrate this more clearly (Fig. 7b), where large fluctuations in intensity are observed in the side view, with a maximum at every 45°, whereas the intensity in the top view remains almost constant. This configuration is retained until the sample is heated above the glass-transition temperature, at

Fig. 7 | Polarizing optical microscopy of shape-programmed PDLCEs. **a** LCE particles assume a disk-like shape after shape programming—a circular geometry is seen from the top view (left), and an elongated geometry from the side view (right). Rotating the sample under crossed polarizers shows no intensity change from the top, but a clear drop in intensity is observed from the side, when the particles are oriented at 45° angles to the polarizers (bottom row; see also Supplementary Fig. 5). **b** The associated polar plot of the sample’s transmittance I/I_0 shows a strong undulation in the side view (red circles) in contrast to the top view (blue circles). **c** The programmed shape of the LCEs (shown in side view) is completely reset to the initial state after thermal cycling over T_{N-I} . The numbers indicate some examples of particle relaxation, zoomed in on the bottom row for better visibility. Scale bars in all images are 100 μm. A retardation plate was used to reduce light scattering for easier distinction between individual microparticles, resulting in a purple background.



which point the particles revert to their original shape and polydomain state (Fig. 7c).

Moreover, due to the uniaxial stress, the disk-shaped particles are consistently aligned with their planes perpendicular to the stress direction. This results in an overall light polarization by the composite when viewed from the two different directions, as indicated by the slight change in background hue (Fig. 7a). This effect disappears after thermal shape resetting (Fig. 7c), when the particles return to their polydomain state and the composite loses its light-polarizing feature.

The strong influence of inclusion geometry on composite mechanical behavior is well known^{37–39}, particularly regarding mechanical anisotropy arising from aligned inclusions, as commonly seen in extruded polymer composites^{40–42}. In our case, the deformation-induced shape change of the LCE particles should contribute significantly to the anisotropic mechanical response of the PDLCE. Thus, the anisotropy in the PDLCEs arises not only from changes in the modulus of the MC-LCE inclusions, but also from their geometry and alignment established during the programming process.

These effects of inclusion geometry and alignment on the effective mechanical properties of composite materials can be estimated using the Halpin–Tsai (HT) equations⁴³, which relate the modulus of the composite to the moduli of the matrix and the inclusions, incorporating the volume fraction, aspect ratio, and geometry of the reinforcing particles. In order to evaluate the magnitude of the particle’s shape on mechanical properties, we therefore apply the same framework to our system.

The Halpin–Tsai equations assume idealized inclusions that are either fully aligned or randomly oriented. In our systems, a fully aligned distribution of disk-shaped LCE microparticles is not realistic, but we use this as a limiting-case approximation to analyze the resulting anisotropic mechanical response. Under this assumption, the Halpin–Tsai equations for the Young’s modulus parallel and transverse to the direction of the shape-programming stress can be expressed as follows^{40,42,43}:

$$E_{\perp} = E_{\text{PDMS}} \frac{1 + \xi \eta \phi}{1 - \eta \phi} \quad (4)$$

and

$$E_{\parallel} = E_{\text{PDMS}} \frac{1 + 2\eta\phi}{1 - \eta\phi} \quad (5)$$

where $\xi = \frac{2}{A} = 2\frac{d}{t}$, $\eta = \frac{E_r - 1}{E_r + \xi}$ and $E_r = \frac{E_{\text{LCE}}}{E_{\text{PDMS}}}$.

Parameter ϕ in the above equations represents the volume fraction of the LCE inclusions. E_{LCE} and E_{PDMS} denote the Young’s moduli of the LCE and PDMS materials, respectively. The parameter $A = t/d$ is the aspect ratio, defined as the ratio between the particle thickness t and the diameter d for disk-shaped inclusions. The HT equations assume that the parallel modulus E_{\parallel} , i.e., modulus measured perpendicular to the aligned disk planes, is equivalent to that of composites with circular inclusions, where the aspect ratio is 1, therefore parameter $\xi = 2$ ^{40,43}.

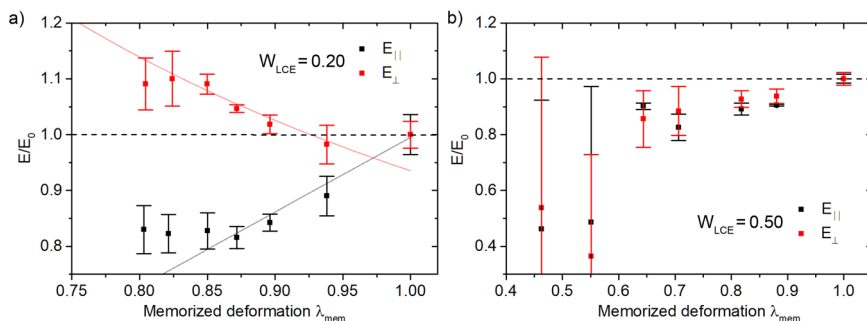
Since the aspect ratio A changes after shape programming depending on the applied programming stress, we aim to express A in terms of the memorized deformation of the LCE fillers, λ_{\parallel}^f , measured along the direction of the programming stress. Assuming that the LCE material is incompressible with a Poisson ratio $\nu = 0.5$ and using the relations $\lambda_{\parallel}^f = t/t_0$ and $\lambda_{\perp}^f = d/d_0$, where t_0 and d_0 are the initial particle thickness and diameter prior to shape programming, it is straightforward to show that:

$$A = A_0 \lambda_{\parallel}^{f\,3/2} \quad (6)$$

Here, the parameter $A_0 = t_0/d_0$ denotes the aspect ratio of the initial particle dimensions. For simplicity, we assume the non-deformed particles are isotropic, and therefore set $A_0 = 1$ in further calculations. In practice, the absolute aspect ratio of the non-programmed particles cannot be reliably defined due to their broad shape distribution, which arises from the cryomilling process and random orientation within the matrix. Rather than relying on particle geometry that is not well-defined, we express the effective aspect ratio in terms of the experimentally measured memorized strain of the composite, λ_{mem} , which inherently captures particle deformation, reorientation, and non-ideal geometry.

The effective shape-memory of the composite is governed by the preserved strain in the LCE inclusions but is reduced due to the elasticity and

Fig. 8 | Mechanical anisotropy in PDLCEs with low and high filler content. **a** PDLCEs with filler content well below percolation still exhibit a high degree of memorized strain and mechanical anisotropy. The modified HT evaluation (solid lines) only partially captures the anisotropic behavior and requires a much higher effective volume fraction ($\phi = 0.832$) than the original amount. **b** PDLCEs with filler content above the percolation level show homogeneous mechanical properties, with a similar reduction in both $E_{||}$ and E_{\perp} . Large experimental errors at higher memorized strains arise from the samples being prone to shear deformations.



lack of memory of the polymer matrix. To relate the memorized deformation of the LCE inclusions, $\lambda_{||}^f$, to that of the PDLCE composite, λ_{mem} , we approximate the PDLCE as a parallel-layered binary composite system (Supplementary Text 2 and Supplementary Fig. 6). For our material composition, specifically due to the high LCE content, the preserved deformation of the PDLCE is demonstrated to be a direct transfer of the LCEs' memorized shape, such that $\lambda_{||}^f \approx \lambda_{mem}$. The aspect ratio of the LCE particles (as defined in Eq. (6)) can therefore be approximated as proportional to the composite's memorized deformation:

$$A \approx \lambda_{mem}^{3/2} \quad (7)$$

We can now directly compare the measured moduli of the programmable PDLCE to the predictions obtained from the Halpin–Tsai model, as presented in Fig. 6. The HT evaluation was calculated from the estimated composite parameters, while volume concentration ϕ was altered to best match the measurements. The material parameters in the HT equations (Eqs. (4) and (5)) were set as $E_{LCE} = 11.4$ MPa, i.e., the average Young's modulus between the measured three sides of the non-deformed LCE material used for the samples (Supplementary Fig. 4) and $E_{PDMS} = 0.823$ MPa obtained from compressive stress-strain measurement of pure PDMS matrix (Supplementary Fig. 7).

The HT approximation (dashed lines in Fig. 6) provides a good fit to the E_{\perp} data for the volume concentration of $\phi = 0.528$, within the expected range for our PDLCE composition. However, the HT model is inadequate for predicting $E_{||}$, due to a known limitation in estimating the Young's modulus parallel to the disk surface^{40,43}. As previously mentioned, the HT equations assume an aspect ratio of 1, which yields a geometrical parameter $\xi = 2$ in this direction.

We acknowledge that changes in particle radius could influence the modulus predictions; however, according to the HT model, if the aspect ratio remains constant, changes in particle radius alone should have little to no effect on the predicted effective modulus. Based on this and supported by POM observations at low particle concentrations (Fig. 7) showing that particles maintain an approximately circular cross-section, we assume that despite the relatively high particle volume fraction and close packing in our composite system, the aspect ratio remains approximately constant (close to 1) with increasing memorized deformation. We therefore propose that the observed changes in $E_{||}$ arises not from geometrical factors, but rather from the increasing anisotropic behavior of the LCE material itself.

Consequently, we modify the classical HT model by rewriting the stiffness ratio $E_r = E_{LCE}/E_{PDMS}$ in HT Eqs. (4) and (5), so that it incorporates the two stretch-moduli components that describe the evolving mechanical anisotropy of the LCE material, as given by Eq. (1). The modified expressions for E_r are:

$$E_r^{||} = \frac{E_{LCE}}{E_{PDMS}} (\lambda_{mem} + s)^2 \quad (8)$$

and

$$E_r^{\perp} = \frac{E_{LCE}}{E_{PDMS}} (\lambda_{mem} + s)^{-2\nu} \quad (9)$$

for the parallel and perpendicular directions, respectively. Because the dispersed LCE particles have no preferred alignment, the original $E_{||}^0$ and E_{\perp}^0 in Eq. (1) are no longer distinguished in the composite and are replaced by the average Young's modulus E_{LCE} . An additional shift parameter s was introduced to adjust the stretch-modulus expressions and account for the lack of domain alignment above a certain strain threshold. Based on the measurements shown in Fig. 3a, no mechanical anisotropy is observed for strains $\lambda_{mem} > 0.87$, and therefore the shift parameter was set to $s = 0.13$.

Using the same material parameters as before, the best fit with the modified HT approximation (full lines in Fig. 6) was achieved with a slightly lower volume concentration of $\phi = 0.515$. The calculations now appear to match the $E_{||}$ measurements quite well. While the trend in E_{\perp} is partially captured, the model tends to overestimate the values. Even if the shift parameter s is set to zero, the model still fails to accurately account for the increase in E_{\perp} . Interestingly, the rise in E_{\perp} begins well before noticeable changes are observed in $E_{||}$.

We thus conclude that, in addition to the inherent limitations of the HT equations, the increase in E_{\perp} is primarily governed by changes in particle geometry, rather than by anisotropy in the Young's modulus. In contrast, $E_{||}$ appears to be more sensitive to mechanical anisotropy, as it is influenced by relatively small or no changes in the overall aspect ratio along this direction. This interpretation is supported by the measurements in Fig. 6, where a noticeable decrease in $E_{||}$ is observed only at deformations above $\lambda_{mem} > 0.87$ — a regime in which the strain is large enough to induce domain realignment, but still too small to significantly affect the geometrical factor. The opposite trend is seen in E_{\perp} , which begins to diverge from the model predictions already at lower memorized deformations, suggesting that it is more strongly influenced by particle shape changes.

The above evaluation is performed on composites with LCE concentrations that exhibit the highest directional TM contraction when magnetically aligned, as shown on the same composites in our previous study². This condition is found at $w_{LCE} = 0.40$. For these systems, as well as for similar PDLCE composites based on side-chain LCEs^{3,44}, we concluded that the highest TM response is achieved around the percolation of LCE particles, where the inclusion concentration is sufficiently high to observe significant TM actuation, while still allowing enough freedom for successful alignment under an external orienting magnetic field.

Regarding shape retention, the percolation level is not expected to play a dominant role, as the degree of shape memory should primarily depend on the amount of filler LCE material. Nevertheless, the mechanical properties of the PDLCE composites are expected to differ in the limiting cases, i.e., well below or well above the percolation level. We have therefore repeated the measurements of the induced mechanical anisotropy for two PDLCEs with low ($w_{LCE} = 0.20$) and high ($w_{LCE} = 0.50$) LCE content (Fig. 8).

The low-content system appears to exhibit behavior somewhat similar to that of its $w_{\text{LCE}} = 0.40$ counterpart. It shows a comparable degree of anisotropy and, somewhat unexpectedly, also retains a high degree of programmed deformation, with $\lambda_{\text{mem}} \approx 0.80$. However, the evolution of E_{\parallel} and E_{\perp} is now reversed compared to the $w_{\text{LCE}} = 0.40$ case: E_{\parallel} decreases significantly at low memorized strain, while E_{\perp} remains nearly constant until $\lambda_{\text{mem}} < 0.90$. Both moduli saturate for $\lambda_{\text{mem}} < 0.85$, resulting in further increases in memorized strain without additional changes in mechanical anisotropy.

At very low filler concentrations, the particles therefore appear to deform more freely in the perpendicular direction, adopting a highly anisotropic shape already at lower programming strains, as evidenced by the immediate drop in E_{\parallel} and the large λ_{mem} . An increase in E_{\perp} would also be expected, however the low particle content likely leads to a reduced effective modulus, possibly due to translational or rotational movements of the now disk-like particles. In contrast to the $w_{\text{LCE}} = 0.40$ system, saturation of both moduli is observed, which may indicate that the particles reach their maximum aspect ratio change for $\lambda_{\text{mem}} < 0.85$.

To assess whether this behavior can be captured within a classical composite framework, we attempted to apply the modified HT equations to gain additional insight into the memory–anisotropy relationship. We were able to partially capture the observed behavior at a volume fraction of $\phi = 0.832$, with an average LCE modulus of $E_{\text{LCE}} = 5.53$ MPa and by adjusting the shift parameter to $s = 0.03$ (solid lines in Fig. 8a). The modified HT equations therefore reproduce the initial composite response only when using a substantially higher effective filler concentration than the nominal value. This indicates that the mechanical response in this regime is governed by deformation-induced filler dominance rather than by the actual inclusion volume fraction, reflecting the high proportion of the easily deformable soft matrix.

The fitted filler concentration should thus be regarded as an effective parameter reflecting enhanced filler–filler interactions and reduced matrix load transfer under compression. In general, the validity of the HT equations relies on efficient matrix–filler load transfer^{40,43} and they are therefore commonly applied to composites with moderate filler concentrations, often below or close to the percolation threshold. As observed for PDLCEs with $w_{\text{LCE}} = 0.40$, the load transfer is closer to a combined contribution from both the LCE filler and the matrix material and the model in this case more accurately reflects the composite's mechanical response using realistic material parameters.

At filler contents above the percolation level (Fig. 8b), the mechanical response differs substantially from that observed at lower filler contents. The composite almost completely memorizes the programmed deformation ($\lambda_{\text{mem}} \approx 0.47$ at maximum $\lambda_{\text{prog}} = 0.40$) and rather than an increase in mechanical anisotropy, a similar reduction in both directional moduli is observed. Both moduli saturate for $\lambda_{\text{mem}} < 0.70$, while at memorized strains $\lambda_{\text{mem}} < 0.65$ the sample becomes highly susceptible to shear deformation, preventing accurate determination of the moduli. Under these conditions, the HT equations are no longer applicable.

Above the percolation level, the mechanical properties of the PDLCE can therefore be considered more homogeneous due to the limited interparticle space, which hinders deformation into uniform, disk-like shapes. The reduction in the moduli likely originates from a soft-elastic response of this polydomain-like system. At the investigated concentrations, however, direct distinction between particle shape and polydomain structure is not possible using optical microscopy. Imaging techniques, such as NMR imaging, could therefore provide valuable insight into these systems.

Discussion

In this study, we prepared a cube-shaped polydomain main-chain LCE sample by cutting it from bulk-synthesized material. Equivalent PDLCE samples containing the same LCE material were molded for comparison. Both materials exhibited effective shape fixation when programmed using thermal cycling under constant compressive load or programming strain.

We successfully instilled varying levels of mechanical anisotropy in individual samples and measured their mechanical properties under compressive stress at room temperature in all three directions. After testing, the programmed shape and anisotropy could be erased by heating and reprogrammed as needed.

In LCEs, the applied compressive stress reorients the mesogens transversely, resulting in a negative order parameter, which was evaluated based on the measured mechanical anisotropy. This anisotropy is reflected in a reduced Young's modulus along the programming direction and an increased modulus perpendicular to it. The theoretical predictions taken from³⁴ align well with the measured directional moduli, even though the LCE was tested in its glass phase.

In PDLCEs, the composite's mechanical anisotropy originates from the deformation of LCE inclusions, which transform from an isotropic to a disk-like geometry under memorized deformation. These inclusions also exhibit transverse mesogen alignment, consistent with the negative ordering observed in the deformed bulk LCE, as confirmed by POM. The two moduli diverge in a similar manner to the parent LCE at moderate concentrations of $w_{\text{LCE}} = 0.40$ and below, though to a lesser extent along the programmed direction. The PDLCE's mechanical anisotropy was analyzed using a modified Halpin–Tsai approach, which suggests that the parallel Young's modulus is more sensitive to increasing mechanical anisotropy of the LCE domains, while the perpendicular modulus is primarily influenced by changes in particle geometry.

The interparticle distance strongly affects the susceptibility of the inclusions to shape programming, as shown by measurements of PDLCEs with concentrations well below and above the percolation level. Below percolation, a highly anisotropic system can still be programmed, whereas above percolation the close packing of particles prevents the establishment of well-defined particle shape order, thereby suppressing mechanical anisotropy. Such high-content PDLCEs can be exploited for designing shape-memory materials that retain an isotropic mechanical response even after shape programming.

Overall, these results demonstrate that PDLCEs not only adopt the TM and shape-memory properties of the parent LCE material^{2,3,36}, but also preserve directional mechanical properties. Given that the composites can contain as little as 20 wt% LCE content to retain comparable shape-memory performance, and around 40 wt% for TM actuation characteristics, they represent a cost-effective platform for achieving programmable materials. Furthermore, compressive programming is more readily achieved in PDLCEs due to their softer nature and more accurate molding.

Further studies could include methods such as NMR spectroscopy or X-ray diffraction to quantify the order parameter imprinted after shape programming in both LCEs and PDLCEs, while imaging techniques like NMR imaging could assist in determining particle geometry at higher LCE concentrations. Beyond the specific LCE and PDLCE systems investigated here, composites incorporating shape-memory or otherwise reprogrammable inclusions remain relatively unexplored. While Tg-driven stiffness changes would provide a general route to relaxation arrest and shape fixation, the magnitude and nature of the resulting mechanical anisotropy remain strongly dependent on changes in particle geometry, as well as on the intrinsic anisotropic properties of the inclusions. In this context, LCEs remain distinct due to their soft elasticity arising from mesogen domain reorientation, which enables particularly large and persistent anisotropic responses. It would therefore be of interest to explore whether comparable levels of intrinsic mechanical anisotropy can be achieved in other composites with shape-programmable inclusions. Together with the suggested approaches above, these studies could further clarify the influence of transverse mesogen alignment in LCEs on the overall thermomechanical behavior of such composite systems.

Methods

Liquid crystal elastomer preparation

Main-chain LCE material (MC-LCE) was prepared by mixing 1.2 mol of 1,1,3,3-tetramethyldisiloxane (used as a flexible chain extender) and

0.08 mol of 2,4,6,8,10-pentamethylcyclopentasiloxane crosslinker with 1 mol of divinyl-terminated mesogenic monomers in a glass flask. The mesogenic monomers were synthesized according to the procedure described in ref. 45. Detailed characterization of the components is available in ref. 2. The mixture was dissolved in 1.3 ml of anhydrous toluene at 343 K, then cooled to room temperature, after which 30 μ l of a platinum catalyst solution, prepared by dissolving (1,5-cyclooctadiene)platinum dichloride in dichloromethane (71 mmol/l), was added. All chemicals were purchased from Sigma-Aldrich and used as received.

The resulting MC-LCE mixture was transferred into an open cylindrical PTFE flask and crosslinked in an oven at 343K over two days to ensure complete evaporation of the solvent. The crosslinked polydomain MC-LCE retained the crude cylindrical shape of the PTFE flask. Cube-shaped samples with side lengths of 2.0 ± 0.2 mm were cut from sections of the material using a scalpel. Cutting was performed on a hot plate heated to 323 K, at which the material becomes slightly softer and easier to handle. Each sample surface was color-marked with a pen to preserve orientation between samples and measurements. After cutting, samples were inspected for imperfections such as cracks or cavities, and only those with a homogeneous structure were selected for TM measurements.

Polymer-dispersed liquid crystal elastomer preparation

PDLCEs were prepared from the same batches and leftover polydomain MC-LCE material used for producing the cube-shaped samples. The MC-LCE was further cut into smaller pieces by using the same procedure as described above (< 1 mm³) and mixed with polydimethylsiloxane, Sylgard® 184 Silicone Elastomer Kit (PDMS), at an LCE weight ratio of $w_{\text{LCE}} = 0.40$ and additional $w_{\text{LCE}} = 0.50$ for production of PDLCEs with low and high LCE content. The mixture was then freeze-fractured using a CryoMill (Retsch GmbH). Milling parameters were as follows: 2 min of pre-cooling at 5 Hz, followed by four intervals of 3 min milling at 30 Hz, each separated by 30 s of intermediate cooling at 5 Hz. The total effective milling time amounted to 12 min. The resulting mixture was scraped from the milling cylinder and mixed at 363 K to form a liquid and homogeneous suspension.

Cube-shaped PDLCE composites were prepared by adding the PDMS curing agent to the PDLCE dispersion at a 1:40 ratio (curing agent to PDMS). For PDLCEs with $w_{\text{LCE}} = 0.20$, the dispersion was appropriately diluted beforehand with additional PDMS. The dispersion was introduced into a rectangular PTFE mold, evacuated to remove any air bubbles, and cured in an oven at 343 K overnight. The dimensions of the resulting strip-shaped PDLCE composite were approximately 20.0 mm \times 6.0 mm \times 2.0 mm. A 2.0 mm-wide block was always cut from one end of the strip and divided into three cube-shaped samples (2.0 ± 0.2 mm per side), which were then used for TM measurements. The sides of the PDLCE samples were marked with different colored pens to preserve their original orientation.

Stress–strain measurements

Measurements of stress–strain properties were performed using a home-built extensometer (Supplementary Fig. 8). The device consists of a temperature-controlled chamber in which the sample is positioned centrally between two cylindrical, piston-like holders. The sample rests on the bottom stationary holder, which is connected to a strain gauge, while the upper holder is mounted on a translator stage. The extensometer is designed to measure the applied stress in response to the position of the upper holder at the desired temperature. Shape-programmed samples were reshaped either by applying a constant stress and thermally cycling the sample in the extensometer to record the process, or by compressing the sample to the desired dimensions using callipers while heating it with a heat gun set to 473 K, followed by natural cooling under constant compression to room temperature. The dimensions of the programmed samples were precisely measured from all sides with the extensometer before testing.

In cases where a good contact between the programmed LCE samples and the holder could not be achieved, the sample was either further cut with a scalpel or its surface was smoothened by briefly rubbing it against a hot plate at 323 K. The latter method proved effective, and no difference in the

measured Young's modulus was observed between cut and temperature-smoothened samples. Due to the softer and more elastic nature of PDLCEs, surface smoothing by heating was not effective, and PDLCE samples were always cut to achieve an even and smooth surface. Mechanical anisotropy was determined from Young's modulus values, derived from stress–strain measurements performed along all three sides of the cube-shaped samples. All tests were conducted at room temperature (300 K), with both materials stressed up to the maximum load permitted by the strain gauge, typically around $\sigma = 650$ kPa. The Young's modulus was determined by applying a linear fit, $\sigma = E\epsilon + k$, within the stress range of 400 – 550kPa.

Temperature-resolved Young's modulus was measured by heating and cooling the samples between 293 K and 423 K and performing stress–strain measurements at each temperature step of 5K or smaller within the glassy-to-nematic transition range (up to 323 K), and in 10 K increments outside this range. The applied loads were the same as those used for the mechanical anisotropy measurements. A minimal load of $\sigma = 2.5$ kPa was applied during temperature changes to prevent any tilting of the sample, and a 5-min waiting time was used after each temperature step before measurement. The Young's modulus was measured in the parallel direction and in one randomly chosen perpendicular direction, since the two perpendicular components are equivalent, as confirmed by the results presented throughout this study. In all cases, measurements were performed at least three times per sample and further compiled from multiple measurements on different samples (up to five), cut from at least two independent synthesis batches.

Thermomechanical measurements

Thermomechanical measurements were performed using the same device as for the stress–strain experiments. Shape programming and strain relaxation were recorded by thermally cycling the sample between 293 K to 423 K at a heating rate of 0.2K/min, under a constant applied compressive load. A load of $\sigma = 245$ kPa was applied for MC-LCEs and $\sigma = 196$ kPa for PDLCEs during the first thermal cycle to record the shape-programming curve. After this cycle, the load was reduced to approximately $\sigma \approx 10$ kPa to allow the sample to relax back toward its initial geometry during the second thermal cycle. For perpendicular shape relaxation measurements, the sample was first shape-programmed under the same load as for the parallel direction, and only the relaxation in the perpendicular direction was recorded.

Optical microscopy

All microscopy images were obtained using a Nikon Eclipse E600 optical polarizing microscope. For this purpose, a low-concentration PDLCE sample with $w_{\text{LCE}} = 0.005$ was prepared, shape-programmed, and then cut into thin sections (< 0.2 mm) in the direction perpendicular or parallel to the programming stress. The very low concentration was necessary to prevent particle overlap during optical observation. Thermomechanical relaxation measurements were performed using an Instec heating stage, with the sample thermally cycled between room temperature and 423 K.

Angular-dependent transmittance was measured on the same samples. The sample was rotated in 5° steps for the side view and 10° steps for the top view, with a greyscale photograph taken at each step. Transmittance I/I_0 was calculated from the total image intensity (I), normalized by the mean intensity of the whole image set (I_0).

Data availability

Raw data generated in this study are available at <https://doi.org/10.6084/m9.figshare.29986360.v1>. Materials and additional data are available from the authors.

Received: 26 August 2025; Accepted: 21 February 2026;

Published online: 01 April 2026

References

1. Warner, M. & Terentjev, E. M. *Liquid Crystal Elastomers*. (Oxford University Press, USA, 2003).

2. Bobnar, M. et al. Polymer-dispersed liquid crystal elastomers as moldable shape-programmable material. *Nat. Commun.* **14**, 764 (2023).
3. Rešetič, A., Milavec, J., Zupančič, B., Domenici, V. & Zalar, B. Polymer-dispersed liquid crystal elastomers. *Nat. Commun.* **7**, 13140 (2016).
4. Asgari, E., Robichaud, A., Cicek, P.-V. & Shih, A. Liquid crystal elastomers in soft micro electromechanical systems: a review of recent developments. *J. Mater. Chem. C* **12**, 15359–15381 (2024).
5. Nie, Z.-Z., Wang, M. & Yang, H. Self-sustainable autonomous soft actuators. *Commun. Chem.* **7**, 58 (2024).
6. Gao, J., Wang, K., Yang, Y. & Feng, W. Self-sustained soft robots based on liquid crystal elastomers. *J. Mater. Chem. C* **13**, 8425–8442 (2025).
7. Herbert, K. M. et al. Synthesis and alignment of liquid crystalline elastomers. *Nat. Rev. Mater.* **7**, 23–38 (2022).
8. Rešetič, A. Shape programming of liquid crystal elastomers. *Commun. Chem.* **7**, 56 (2024).
9. Lan, R. et al. Adaptive liquid crystal polymers based on dynamic bonds: from fundamentals to functionalities. *Responsive Mater.* **2**, e20230030 (2024).
10. Das, G. & Park, S.-Y. Liquid crystalline elastomer actuators with dynamic covalent bonding: synthesis, alignment, reprogrammability, and self-healing. *Curr. Opin. Solid State Mater. Sci.* **27**, 101076 (2023).
11. Ohzono, T., Katoh, K., Minamikawa, H., Saed, M. O. & Terentjev, E. M. Internal constraints and arrested relaxation in main-chain nematic elastomers. *Nat. Commun.* **12**, 787 (2021).
12. Chen, G. et al. Rapidly and repeatedly reprogrammable liquid crystalline elastomer via a shape memory mechanism. *Adv. Mater.* **34**, 2201679 (2022).
13. Lendlein, A. & Gould, O. E. C. Reprogrammable recovery and actuation behaviour of shape-memory polymers. *Nat. Rev. Mater.* **4**, 116–133 (2019).
14. Aßfalg, N. & Finkelmann, H. A smectic a liquid single crystal elastomer (LSCE): phase behavior and mechanical anisotropy. *Macromol. Chem. Phys.* **202**, 794–800 (2001).
15. Merkel, D. R. et al. Thermomechanical properties of monodomain nematic main-chain liquid crystal elastomers. *Soft Matter* **14**, 6024–6036 (2018).
16. Mistry, D. & Gleeson, H. F. Mechanical deformations of a liquid crystal elastomer at director angles between 0° and 90°: deducing an empirical model encompassing anisotropic nonlinearity. *J. Polym. Sci. Part B.* **57**, 1367–1377 (2019).
17. Oh, S.-W. et al. Measuring the five elastic constants of a nematic liquid crystal elastomer. *Liq. Cryst.* **48**, 511–520 (2021).
18. Okamoto, S., Sakurai, S. & Urayama, K. Effect of stretching angle on the stress plateau behavior of main-chain liquid crystal elastomers. *Soft Matter* **17**, 3128–3136 (2021).
19. Tokumoto, H. et al. Probing the in-plane liquid-like behavior of liquid crystal elastomers. *Sci. Adv.* **7**, eabe9495 (2021).
20. Gang, Y. et al. On the origin of elasticity and heat conduction anisotropy of liquid crystal elastomers at gigahertz frequencies. *Nat. Commun.* **13**, 5248 (2022).
21. R. Berrow, S. et al. The effect of templating on the mechanical properties of smectic liquid crystal elastomers. *J. Mater. Chem. C* **13**, 12365–12375 (2025).
22. Weilepp, J. et al. Rheology of liquid crystalline elastomers in their isotropic and smectic A state. *Macromolecules* **32**, 4566–4574 (1999).
23. Wang, M. et al. A liquid crystal elastomer-based unprecedented two-way shape-memory aerogel. *Adv. Sci.* **8**, 2102674 (2021).
24. Song, B. et al. On the effect of strain rate during the cyclic compressive loading of liquid crystal elastomers and their 3D printed lattices. *Mech. Mater.* **197**, 105086 (2024).
25. Agrawal, A. et al. Dynamic self-stiffening in liquid crystal elastomers. *Nat. Commun.* **4**, 1739 (2013).
26. Mistry, D. et al. Coincident molecular auxeticity and negative order parameter in a liquid crystal elastomer. *Nat. Commun.* **9**, 5095 (2018).
27. He, Y. et al. 4D printing of polymer-dispersed liquid crystal elastomers toward tunable vibration isolation and cushioning properties. *Adv. Mater. Technol.* **10**, e00078 (2025).
28. Lorthioir, C., Deloche, B. & Courtieu, J. Experimental evidence for a negative orientational order parameter in a uniaxially compressed poly(dimethylsiloxane) network. *Macromolecules* **34**, 8835–8837 (2001).
29. Jampani, V. S. R. et al. Liquid crystal elastomer shell actuators with negative order parameter. *Sci. Adv.* **5**, eaaw2476 (2019).
30. Traugott, N. A. et al. Liquid-crystal-elastomer-based dissipative structures by digital light processing 3D printing. *Adv. Mater.* **32**, 2000797 (2020).
31. Mistry, D. et al. Soft elasticity optimises dissipation in 3D-printed liquid crystal elastomers. *Nat. Commun.* **12**, 6677 (2021).
32. Bischoff, A. et al. Monodomain liquid-crystal elastomer lattices for broad strain-rate mechanical damping. *Adv. Eng. Mater.* **27**, 2401796 (2025).
33. Zhao, S., Chen, Y. & Huo, Y. Formation of lamellar domains in liquid crystal elastomers under compression. *Int. J. Mech. Sci.* **247**, 108185 (2023).
34. Mihai, L. A., Wang, H., Guilleminot, J. & Goriely, A. Nematic liquid crystalline elastomers are aeolotropic materials. *Proc. R. Soc. A* **477**, 20210259 (2021).
35. Milavec, J. et al. Deuteron NMR resolved mesogen vs. crosslinker molecular order and reorientational exchange in liquid single crystal elastomers. *Phys. Chem. Chem. Phys.* **18**, 4071–4077 (2016).
36. Umerova, S. et al. Shear flow-controlled shape memory of polymer resin dispersed liquid crystal elastomer microparticles. *Mater. Des.* **207**, 109836 (2021).
37. Chow, T. S. The effect of particle shape on the mechanical properties of filled polymers. *J. Mater. Sci.* **15**, 1873–1888 (1980).
38. Chow, T. S. Prediction of stress-strain relationships in polymer composites. *Polymer* **32**, 29–33 (1991).
39. Rakow, J. F. & Waas, A. M. The effective isotropic moduli of random fibrous composites, platelet composites, and foamed solids. *Mech. Adv. Mater. Struct.* **11**, 151–173 (2004).
40. Brune, D. A. & Bicerano, J. Micromechanics of nanocomposites: comparison of tensile and compressive elastic moduli, and prediction of effects of incomplete exfoliation and imperfect alignment on modulus. *Polymer* **43**, 369–387 (2002).
41. Verbeek, C. J. R. & Focke, W. W. Modelling the Young's modulus of platelet reinforced thermoplastic sheet composites. *Compos. Part A* **33**, 1697–1704 (2002).
42. Mortazavian, S. & Fatemi, A. Effects of fiber orientation and anisotropy on tensile strength and elastic modulus of short fiber reinforced polymer composites. *Compos. Part B* **72**, 116–129 (2015).
43. Afdl, J. C. H. & Kardos, J. L. The Halpin-Tsai equations: a review. *Polym. Eng. Sci.* **16**, 344–352 (1976).
44. Rešetič, A. et al. Deuteron NMR investigation on orientational order parameter in polymer dispersed liquid crystal elastomers. *Phys. Chem. Chem. Phys.* **22**, 23064–23072 (2020).
45. Bispo, M., Guillon, D., Donnio, B. & Finkelmann, H. Main-chain liquid crystalline elastomers: monomer and cross-linker molecular control of the thermotropic and elastic properties. *Macromolecules* **41**, 3098–3108 (2008).

Acknowledgements

This work was supported by the Slovenian Research and Innovation Agency (ARIS), research program P1-0125.

Author contributions

A.R. defined the initial research directions and supervised the study. V.D. and A.R. synthesized main-chain mesogen components, liquid crystal elastomers and polymer-dispersed liquid crystal elastomers. M.L., L.R.K. and A.R. performed the experiments and analyzed the data. M.L. and L.R.K. prepared the data representation and graphics. A.R. wrote the main paper text, with contributions from all authors.

Competing interests

The authors declare no competing interests.

Additional information

Supplementary information The online version contains supplementary material available at

<https://doi.org/10.1038/s44431-026-00022-z>.

Correspondence and requests for materials should be addressed to Andraž. Rešetič.

Reprints and permissions information is available at <http://www.nature.com/reprints>

Publisher's note Springer Nature remains neutral with regard to jurisdictional claims in published maps and institutional affiliations.

Open Access This article is licensed under a Creative Commons Attribution 4.0 International License, which permits use, sharing, adaptation, distribution and reproduction in any medium or format, as long as you give appropriate credit to the original author(s) and the source, provide a link to the Creative Commons licence, and indicate if changes were made. The images or other third party material in this article are included in the article's Creative Commons licence, unless indicated otherwise in a credit line to the material. If material is not included in the article's Creative Commons licence and your intended use is not permitted by statutory regulation or exceeds the permitted use, you will need to obtain permission directly from the copyright holder. To view a copy of this licence, visit <http://creativecommons.org/licenses/by/4.0/>.

© The Author(s) 2026